

QCD Dirac operator at nonzero chemical potential: lattice data and matrix model

Gernot Akemann

*Service de Physique Théorique, CEA/DSM/SPhT Saclay,
Unité de recherche associée au CNRS, F-91191 Gif-sur-Yvette Cedex, France*

Tilo Wettig

*Department of Physics, Yale University, New Haven, CT 06520-8120, USA and
RIKEN-BNL Research Center, Brookhaven National Laboratory, Upton, NY 11973-5000, USA
(Dated: August 4, 2003)*

Recently, a nonhermitian chiral random matrix model was proposed to describe the eigenvalues of the QCD Dirac operator at nonzero chemical potential. This matrix model can be derived directly from QCD by mapping it to an equivalent matrix model which has the same symmetries as QCD with chemical potential. Its microscopic spectral correlations are conjectured to be identical to those of the QCD Dirac operator. We investigate this conjecture by comparing large ensembles of Dirac eigenvalues in quenched SU(3) lattice QCD at nonzero chemical potential to the analytical predictions of the matrix model. Excellent agreement is found in the two regimes of weak and strong nonhermiticity, for several different lattice volumes.

PACS numbers: 12.38.Gc, 02.10.Yn

There has been a lot of recent interest in physical systems described by nonhermitian operators. Such operators play a rôle in many areas of physics, e.g., S-matrix theory [1], dissipative quantum maps [2], neural network dynamics [3], disordered systems with imaginary vector potential [4], and quantum chromodynamics (QCD) at nonzero density [5]. In the present work, we are mainly interested in the last of these applications, but we expect the matrix model to be described below to be applicable to nonhermitian operators in other physical systems as well, provided they are in the same symmetry class.

QCD at nonzero density is important in a variety of physical situations, such as relativistic heavy-ion collisions or neutron stars. Considerable progress has been made in the last few years on the analytical side. For example, the regime of asymptotically large density is well understood [6], and qualitative predictions for the QCD phase diagram could be derived on the basis of symmetry considerations [7]. However, we would really like to be able to compute quantitative results at physically relevant densities. Unfortunately, lattice simulations of full QCD at nonzero chemical potential μ are extremely difficult: the weight function is complex, and the numerical effort increases exponentially with the volume. A number of interesting new ideas have recently been investigated on the lattice side, e.g., reweighting along the critical line [8], combined expansions of weight function and observable [9], analytic continuation from imaginary μ [10], and a factorization method for distribution functions of observables [11]. It is questionable, however, whether these techniques will allow us to approach the thermodynamic limit.

Clearly, a better theoretical understanding of QCD at nonzero density is desirable. The Dirac operator is one of the central objects in QCD. Many observables can be

expressed in terms of its eigenvalues and eigenvectors. While much is known about this eigenvalue spectrum at $\mu = 0$ (see Ref. [12] for a review), the situation at $\mu \neq 0$ is less satisfying. The goal of the present work is to improve our understanding of the latter case. We concentrate on a particular matrix model for the QCD Dirac operator at nonzero μ and show that its analytical predictions for the distribution of small Dirac eigenvalues are in agreement with data from lattice gauge simulations. This statement holds in the two different regimes of weak and strong nonhermiticity, to be defined below. The implications of these results are discussed in the conclusions.

We start by presenting the matrix model and its predictions [13]. The model constitutes a complex extension of the chiral Gaussian Unitary Ensemble (GUE) [14]. In terms of the complex eigenvalues z_j ($j = 1, \dots, N$), its partition function reads

$$Z_\nu(\tau; \{m_f\}) = \int_{\mathbb{C}} \prod_{j=1}^N dz_j dz_j^* |z_j|^{2|\nu|+1} \prod_{f=1}^{N_f} (z_j^2 + m_f^2) \times e^{-\frac{N}{1-\tau^2} [|z_j|^2 - \frac{\tau}{2} (z_j^2 + z_j^{*2})]} \prod_{k>l}^N |z_k^2 - z_l^2|^2 \quad (1)$$

for N_f flavors of masses m_f ($f = 1, \dots, N_f$) in the sector of topological charge ν . The parameter $\tau \in [0, 1]$ measures the degree of nonhermiticity and is related to μ by

$$2\mu^2 = 1 - \tau^2. \quad (2)$$

In the limit $\tau \rightarrow 1$ (or $\mu \rightarrow 0$), the eigenvalues are real and we are back to the chiral GUE. For $\tau \rightarrow 0$ the nonhermiticity is maximal, and the model becomes a chiral extension of the Ginibre Ensemble [15]. The relation (2) follows from comparing the current model to the matrix

model of Ref. [5] at small μ . That model is defined by

$$\hat{Z}_\nu(\mu; \{m_f\}) = \int_{\mathbb{C}^{(N+\nu) \times N}} d\Phi \prod_{f=1}^{N_f} \det \begin{bmatrix} m_f & i\Phi + \mu \\ i\Phi^\dagger + \mu & m_f \end{bmatrix} \times \exp[-N \text{Tr} \Phi^\dagger \Phi] \quad (3)$$

and has the same global symmetries as QCD. The current model (1) is equivalent to the model (3) at the level of the partition function for small values of μ [16]. (However, unlike the model (3), it is always in the phase with broken chiral symmetry.) It has not yet been possible to compute the microscopic spectral correlations (i.e., the correlations of the smallest eigenvalues on the scale of the mean level spacing) for model (3). In contrast, this has been achieved for model (1) in Ref. [13], and it is conjectured that the two models, as well as QCD, are in the same universality class in the sense that they yield identical results for the microscopic spectral correlations.

Explicit analytical predictions can be derived from the model (1) at large N using the technique of orthogonal polynomials in the complex plane [13]. So far results have been obtained for $N_f = 0$ and N_f phase quenched massless flavors, replacing $|\nu| \rightarrow |\nu| + N_f$. Two different large- N limits have to be distinguished. In the limit of weak nonhermiticity [17], the product

$$\lim_{N \rightarrow \infty} \lim_{\tau \rightarrow 1} N(1 - \tau^2) = \lim_{N \rightarrow \infty} \lim_{\mu \rightarrow 0} 2N\mu^2 \equiv \alpha^2 \quad (4)$$

is kept fixed. This corresponds to taking the volume $V \propto N$ to infinity such that $V\mu^2$ is fixed. The result of the current model in this limit for the density of small Dirac eigenvalues reads (using $N_f = 0$ corresponding to the quenched limit appropriate for our lattice data)

$$\rho_{\text{weak}}(\xi) = \frac{\sqrt{\pi\alpha^2}}{\text{erf}(\alpha)} |\xi| \exp\left[-\frac{(\Im m \xi)^2}{\alpha^2}\right] \times \int_0^1 dt e^{-\alpha^2 t} J_{|\nu|}(\sqrt{t}\xi) J_{|\nu|}(\sqrt{t}\xi^*), \quad (5)$$

where J denotes the Bessel function and the eigenvalues have been rescaled according to $\xi = Nz\sqrt{2}$.

In the limit of strong nonhermiticity, we send $N \rightarrow \infty$ at fixed $\tau \in [0, 1)$ and obtain

$$\rho_{\text{strong}}(\xi) = \sqrt{\frac{2\pi}{1-\tau^2}} |\xi| \exp\left[\frac{-|\xi|^2}{1-\tau^2}\right] I_{|\nu|}\left(\frac{|\xi|^2}{1-\tau^2}\right), \quad (6)$$

where I denotes the modified Bessel function and we have rescaled $\xi = \sqrt{N}z$. Higher-order spectral correlations have also been computed in both limits for $\nu \neq 0$ in [13], but they are not the subject of the present work.

We stress that the existence of these two different scaling regimes is a prediction for the lattice, and we will indeed identify these two regimes in the data below.

We now turn to the details of the lattice simulations and discuss some of the concerns arising from our choices

of operator and simulation parameters. We use the staggered Dirac operator, given at $\mu \neq 0$ by [18]

$$D_{x,y}(U, \mu) = \frac{1}{2} \sum_{\nu=\hat{x},\hat{y},\hat{z}} [U_\nu(x)\eta_\nu(x)\delta_{y,x+\nu} - \text{h.c.}] + \frac{1}{2} [U_{\hat{t}}(x)\eta_{\hat{t}}(x)e^\mu\delta_{y,x+\hat{t}} - U_{\hat{t}}^\dagger(y)\eta_{\hat{t}}(y)e^{-\mu}\delta_{y,x-\hat{t}}], \quad (7)$$

where the $U_\nu(x)$ are SU(3) gauge fields, the $\eta_i(x)$ are the staggered phases, and the lattice spacing has been set to unity. For convenience, we shall denote its eigenvalues by $i\lambda_k$ so that at $\mu = 0$ the λ_k are real. The reason to prefer the staggered Dirac operator over other formulations is that (a) the Wilson operator breaks chiral symmetry explicitly and has complex eigenvalues even at $\mu = 0$, and (b) Ginsparg-Wilson-type operators are much more expensive to compute, which is a serious issue here because we need many configurations (see Table I).

The gauge field configurations were generated in the quenched approximation, corresponding to $N_f = 0$. The fact that this approximation is unphysical [5] does not constitute a problem for the present work. Our primary interest is in testing the predictions of the matrix model (1). If the results of the model agree with the lattice data for $N_f = 0$, they should also agree at $N_f \neq 0$ because the matrix model remains valid. This is analogous to the situation at $\mu = 0$ [19]. In fact, the unquenched matrix model has already been used to test algorithms [11].

In the simulations we used $\beta = 6/g^2 = 5.0$, which corresponds to the strong-coupling regime and is far from the continuum limit in which one is ultimately interested. Nevertheless, working at such a low value of β is both convenient and legitimate for the present purpose, for the following reason. The microscopic spectral correlations are described by a random matrix model only below the so-called Thouless energy, which is the boundary of the regime in which the zero-momentum modes dominate the partition function of the low-energy effective theory in a finite volume [12]. The Thouless energy is a function of both β and the lattice volume V . If β is increased at fixed V , fewer Dirac eigenvalues are described by the matrix model. Increasing V works in the opposite direction. Thus, for small β we can test the matrix model on relatively small lattices. At larger values of β we simply need to increase the lattice volume, which, however, is inconvenient numerically.

At this small value of β , the staggered Dirac operator does not have exact zero modes even if the underlying gauge field has nonzero topological charge, because the would-be zero modes are shifted by an amount proportional to the square of the lattice spacing. This amount is much larger than the mean level spacing near zero, and thus the would-be zero modes are completely mixed with the nonzero modes. We account for this by setting $\nu = 0$ in Eqs. (1), (5), and (6). (This “disease” of staggered fermions can be overcome by going to very small lattice spacing [20] or by using the overlap operator [21].)

TABLE I: Summary of simulation parameters (using $\beta = 5.0$).

| V | μ | level spacing d | no. of config. |
|--------|----------|----------------------|----------------|
| 6^4 | 0.006 | $1.99 \cdot 10^{-3}$ | 17,000 |
| 6^4 | 0.03 | $2.21 \cdot 10^{-3}$ | 20,000 |
| 6^4 | 0.2 | $7.57 \cdot 10^{-3}$ | 20,000 |
| 8^4 | 0.003375 | $6.51 \cdot 10^{-4}$ | 20,000 |
| 8^4 | 0.2 | $4.04 \cdot 10^{-3}$ | 20,000 |
| 10^4 | 0.00216 | $2.65 \cdot 10^{-4}$ | 4,000 |
| 10^4 | 0.2 | $2.57 \cdot 10^{-3}$ | 4,000 |

Our simulation parameters are summarized in Table I. In the regime of strong nonhermiticity, we used a constant value of $\mu = 0.2$, whereas for weak nonhermiticity, we varied μ such that the product $\mu^2 V$ is fixed. On the 6^4 lattice, the complete eigenvalue spectrum can be computed on a single PC rather quickly using LAPACK [22]. For the larger lattices we switched to ARPACK [23] and computed only the 100 eigenvalues of smallest absolute magnitude with positive real part (the eigenvalues come in pairs $\pm \lambda_k$). Since ARPACK is very fast at computing the largest eigenvalues, we inverted the Dirac operator prior to feeding it to ARPACK, using the sparse LU solver UMFPACK [24].

Because we are only interested in the small eigenvalues of the Dirac operator, global unfolding of the spectrum [25] is not necessary; we simply rescale the eigenvalues by a constant determined from the mean level spacing d of the data near zero. Note that $d \propto 1/V$.

We first present our results for weak nonhermiticity. Since three-dimensional plots are hard to read, we instead show cuts along the real and imaginary axes. In Fig. 1 the data for lattice size 6^4 and $\mu = 0.006$ are plotted versus Eq. (5). There is no free fit parameter; the

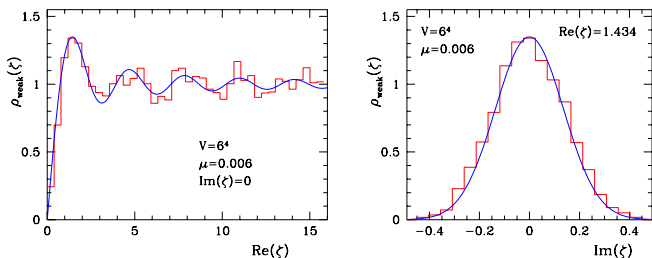


FIG. 1: Density of small Dirac eigenvalues for $V = 6^4$ and $\mu = 0.006$, cut along the real axis (left) and parallel to the imaginary axis at the first maximum (right). The histogram represents lattice data, and the solid curve is Eq. (5).

data have been rescaled according to $\xi = \pi z/d$, with d given in Table I. (The level spacing is conventionally chosen to be π [14] and not unity.) At weak nonhermiticity d can be obtained in the same way as for real eigenvalues: Because of the smallness of their imaginary part the eigenvalues can still be ordered with respect to their real part so that the level spacing is defined unambigu-

ously. The very same level spacing d is used to determine $\alpha^2 = 2\mu^2/d$ from Eq. (4), leading to $\alpha = 0.19$ for use in Eq. (5). We obtain excellent agreement of lattice data and analytical prediction without any free fit parameter. In Fig. 2 we repeat the same analysis for lattice size 8^4

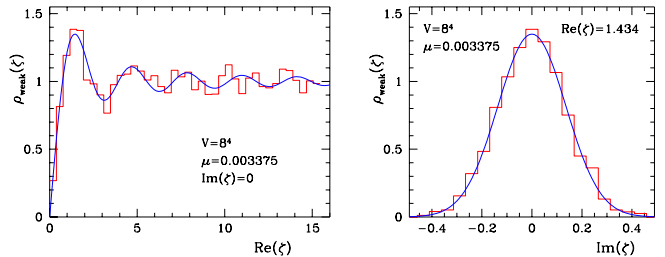


FIG. 2: Same as Fig. 1 but for $V = 8^4$ and $\mu = 0.003375$.

and $\mu = 0.003375$, chosen to keep $V\mu^2 = \alpha^2$ constant in order to test the scaling predicted by Eq. (4). Here we have used the same value of $\alpha = 0.19$ and again find excellent agreement. This value agrees within 1.5% with the value of α determined independently by rescaling μ^2 with the level spacing d from the 8^4 data. Similar results are obtained from the analysis of the 10^4 data which we do not display here because of limited statistics. These findings confirm the analytical prediction of Eq. (5) for the weak-nonhermiticity limit as well as the scaling with $V\mu^2$ for different lattice volumes.

Next we turn to the limit of strong nonhermiticity. Here, the eigenvalues are no longer localized close to the real axis and spread into a two-dimensional domain in the complex plane. The signature of the chiral ensemble (1) compared to the Ginibre ensemble [15] is a “hole” at the origin resulting from the level repulsion near zero. (The latter ensemble applies only in the bulk of the spectrum [25].) In Fig. 3 we plot the data for $V = 6^4$ and $\mu = 0.2$

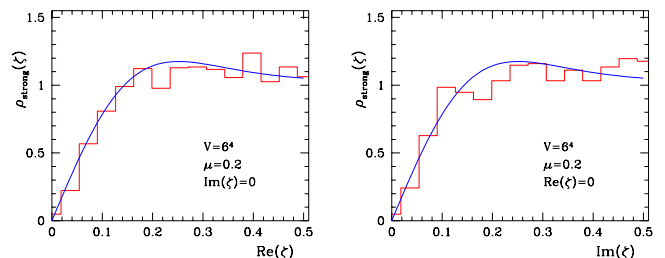


FIG. 3: Density of small Dirac eigenvalues for $V = 6^4$ and $\mu = 0.2$, cut along the real (left) and imaginary (right) axes. The histogram represents lattice data, and the solid curve is the prediction of Eq. (6).

versus the prediction of Eq. (6). The data are now rescaled according to $\xi = \pi z/\sqrt{d}$, taking into account the different volume dependence in the strong limit. The value of τ is obtained from Eq. (2), $\tau = \sqrt{1 - 2\mu^2} \approx 0.96$, without rescaling μ . (Note that the analytic curve is identical along the real and imaginary axes due to its ro-

tational invariance. This is not true for the macroscopic density.) Nice agreement is found, again without any free parameter, but despite using roughly the same number of configurations, the statistical error is larger than in the weak limit. This is due to the fact that the data now substantially fill a two-dimensional surface. Therefore we also have to modify the determination of the mean level spacing d . Nearest neighbors are now defined as having the smallest geometric distance between them. As can be seen from Table I, the level spacing d is very different from the weak limit. This is due to the spreading into the complex plane, as the spacing of the eigenvalues projected onto the real axis remains approximately constant for the values of μ chosen. The same analysis is repeated for lattice size 8^4 and the same value of $\mu = 0.2$, as shown in Fig. 4. We again obtain good agreement, also in the

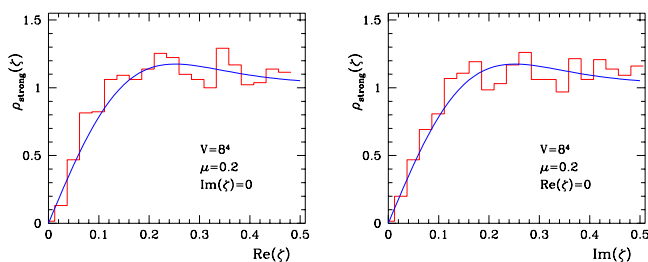


FIG. 4: Same as Fig. 3 but for $V = 8^4$ and $\mu = 0.2$.

case of $V = 10^4$ and $\mu = 0.2$ (not shown).

Note, however, that there is an important difference between the cuts in the real and imaginary directions. While the microscopic density, Eq. (6), is rotationally invariant, the data spread macroscopically into a thin ellipse. Along the imaginary axis the spectrum ends at $\approx \pm 1.1$ in our units, while along the real axis it extends up to $\approx \pm 75$. For that reason the last part of the histograms along the imaginary axis in Figs. 3 and 4 may no longer be in the microscopic regime. In the data for $V = 6^4$ at intermediate $\mu = 0.03$, the microscopic and macroscopic scales no longer separate clearly, and therefore neither of the Eqs. (5) and (6) apply.

In conclusion, we have identified two different regimes in the behavior of the complex eigenvalues of the QCD Dirac operator in the domain where chiral symmetry is broken. Our lattice data confirm the predictions of random matrix theory quantitatively, both at weak and at strong nonhermiticity, without any free parameter. Matrix models thus provide a detailed theoretical understanding of the properties of the complex Dirac eigenvalues in a new regime with non-vanishing chemical potential, including the correct scaling of eigenvalues and chemical potential with the volume. Our findings may have algorithmical implications, since it is typically the low-lying Dirac eigenvalues which determine the numerical effort in lattice simulations. We wish to emphasize

that, although our conclusions are based on quenched simulations using staggered fermions, the predictions of the matrix model could also be tested in unquenched simulations as well as in sectors of nontrivial topological charge. This will be the subject of future work.

This work was supported in part by a Heisenberg fellowship of the DFG (GA) and by DOE grant DE-FG02-91ER40608 (TW).

-
- [1] J.J.M. Verbaarschot, H.A. Weidenmüller, and M.R. Zirnbauer, Phys. Rep. 129 (1985) 367
 - [2] R. Grobe, F. Haake, and H.-J. Sommers, Phys. Rev. Lett. 61 (1988) 1899
 - [3] N. Lehmann and H.-J. Sommers, Phys. Rev. Lett. 67 (1991) 941
 - [4] N. Hatano and D.R. Nelson, Phys. Rev. Lett. 77 (1996) 570, J. Miller and J. Wang, Phys. Rev. Lett. 76 (1996) 1461
 - [5] M.A. Stephanov, Phys. Rev. Lett. 76 (1996) 4472
 - [6] e.g., M. Alford, K. Rajagopal, and F. Wilczek, Nucl. Phys. B 537 (1999) 443 and references therein
 - [7] M.A. Halasz, A.D. Jackson, R.E. Shrock, M.A. Stephanov, and J.J.M. Verbaarschot, Phys. Rev. D 58 (1998) 096007
 - [8] Z. Fodor and S.D. Katz, Phys. Lett. B 534 (2002) 87
 - [9] C.R. Allton et al., Phys. Rev. D 66 (2002) 074507
 - [10] P. de Forcrand and O. Philipsen, Nucl. Phys. B 642 (2002) 290, M. D'Elia and M.-P. Lombardo, Phys. Rev. D 67 (2003) 014505
 - [11] J. Ambjørn, K.N. Anagnostopoulos, J. Nishimura, and J.J.M. Verbaarschot, JHEP 0210 (2002) 062
 - [12] J.J.M. Verbaarschot and T. Wettig, Ann. Rev. Nucl. Part. Sci. 50 (2000) 343
 - [13] G. Akemann, Phys. Rev. Lett. 89 (2002) 072002, J. Phys. A 36 (2003) 3363
 - [14] E.V. Shuryak and J.J.M. Verbaarschot, Nucl. Phys. A 560 (1993) 306; J.J.M. Verbaarschot, Phys. Rev. Lett. 72 (1994) 2531
 - [15] J. Ginibre, J. Math. Phys. 6 (1965) 440
 - [16] G. Akemann, hep-th/0307116
 - [17] Y.V. Fyodorov, B.A. Khoruzhenko, and H.-J. Sommers, Phys. Lett. A 226 (1997) 46, Phys. Rev. Lett. 79 (1997) 557
 - [18] P. Hasenfratz and F. Karsch, Phys. Lett. B 125 (1983) 308
 - [19] M.E. Berbenni-Bitsch, S. Meyer, and T. Wettig, Phys. Rev. D 58 (1998) 071502; G. Akemann and E. Kanzieper, Phys. Rev. Lett. 85 (2000) 1174
 - [20] F. Farchioni, I. Hip, and C.B. Lang, Phys. Lett. B 471 (1999) 58
 - [21] R.G. Edwards, U.M. Heller, J. Kiskis, and R. Narayanan, Phys. Rev. Lett. 82 (1999) 4188
 - [22] www.netlib.org/lapack
 - [23] www.netlib.org/arpac
 - [24] www.cise.ufl.edu/research/sparse/umfpack
 - [25] H. Markum, R. Pullirsch, and T. Wettig, Phys. Rev. Lett. 83 (1999) 484